

Experimental Studies of the Interconversion of μ - η^2 : η^2 -Peroxo- and Bis(μ -oxo)dicopper Complexes

John Cahoy, Patrick L. Holland, and William B. Tolman*

Department of Chemistry and Center for Metals in Biocatalysis, University of Minnesota,
207 Pleasant Street SE, Minneapolis, Minnesota 55455

Received January 20, 1999

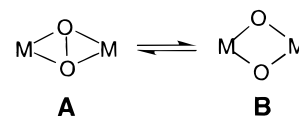
The effects of solvent composition, counterion, and temperature on the equilibrium between the isomeric complexes $[(L^{iPr3}Cu)_2(\mu-\eta^2:\eta^2-O_2)]X_2$ [**1**(X)₂] and $[(L^{iPr3}Cu)_2(\mu-O)_2]X_2$ [**2**(X)₂; $L^{iPr3} = 1,4,7$ -triisopropyl-1,4,7-triazacyclononane; X = PF₆⁻, ClO₄⁻, or SbF₆⁻], which differ with respect to the presence and absence, respectively, of an O–O bond, were examined via solution conductivity and UV–vis and resonance Raman spectroscopic measurements. While previous work (Halfen, J. A.; Mahapatra, S.; Wilkinson, E. C.; Kaderli, S.; Young, V. G., Jr.; Que, L., Jr.; Zuberbühler, A. D.; Tolman, W. B. *Science* **1996**, *271*, 1397–1400) had shown that **2**(X)₂ (X = PF₆⁻ or ClO₄⁻) formed exclusively in THF solution at concentrations >1 mM, new experimental results show that preferential aggregation/precipitation of **2**(X)₂ occurs under these conditions. By using lower concentrations and/or X = SbF₆⁻, apparently homogeneous solutions of mixtures of **1**(X)₂ and **2**(X)₂ in equilibrium in THF and THF/CH₂Cl₂ mixtures are generated. Evaluation of the temperature dependence of the equilibrium in THF allowed estimation of thermodynamic parameters [$\Delta H = 0.9(2)$ kcal mol⁻¹ and $\Delta S = 6(1)$ cal mol⁻¹ K⁻¹] that are consistent with the small energetic differences between analogous isomers previously calculated using theoretical methods. In addition, by avoiding the selective aggregation/precipitation of **2**(X)₂, the **1**(X)₂/**2**(X)₂ equilibrium was shown to exhibit a smooth dependence on the THF:CH₂Cl₂ ratio in solvent mixtures. The observed gradual shifts in the proportion of the equilibrating isomers as a function of solvent and temperature show that subtle environmental factors influence the equilibrium in similarly subtle ways, with implications for the potential involvement of both types of cores in biological and other catalytic processes.

Introduction

An important objective in research aimed at understanding oxidations by metal-containing industrial and biological catalysts is to unravel the mechanism(s) by which the dioxygen O–O bond is broken and substrate C–H bonds are attacked.¹ Of equal importance is understanding how the dioxygen O–O bond is forged, also at a metal-containing site, during photosynthesis.² Studies of well-characterized, discrete synthetic metal complexes have been useful for evaluating the myriad ways by which O–O bond making and breaking may occur in diverse systems.^{1d,3} As recent publications attest, however, we still do not understand

many aspects of the mechanisms by which dioxygen is consumed or generated, particularly by multimetal assemblies.^{1–4}

A possible way that O–O bond breaking and/or making in biological and catalytic systems comprising two (or more) metal ions may proceed is via the interconversion of the μ - η^2 : η^2 -peroxo- and the bis(μ -oxo)dimetal units **A** and **B**. This notion

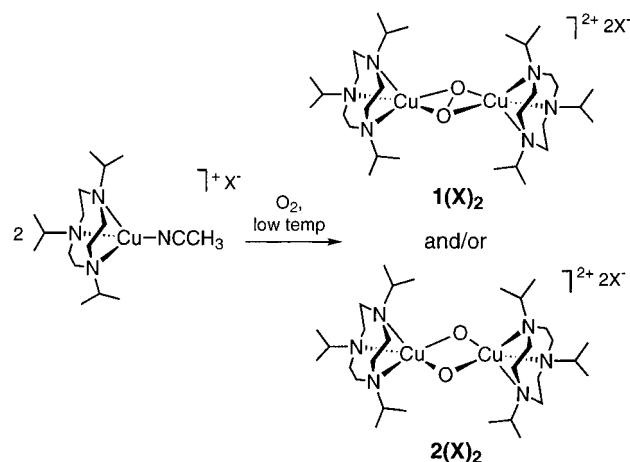


was rendered feasible by the recent discovery of such a process in synthetic copper complexes.^{3g,5} Specifically, treatment of $[L^{iPr3}Cu(CH_3CN)]X$ ($L^{iPr3} = 1,4,7$ -triisopropyl-1,4,7-triazacyclononane; X = PF₆⁻ or SbF₆⁻) in acetone with O₂ at –80 °C formed a ~4:1 mixture of $[(L^{iPr3}Cu)_2(\mu-\eta^2:\eta^2-O_2)]X_2$ [**1**(X)₂,

- (1) Selected publications: (a) Sheldon, R. A.; Kochi, J. K. *Metal-Catalyzed Oxidations of Organic Compounds*; Academic Press: New York, 1981. (b) *Cytochrome P450: Structure, Mechanism, and Biochemistry*, 2nd ed.; Ortiz de Montellano, P. R., Ed.; Plenum Press: New York, 1995. (c) Drago, R. S. *Coord. Chem. Rev.* **1992**, *117*, 185–213. (d) Feig, A. L.; Lippard, S. J. *Chem. Rev.* **1994**, *94*, 759–805. (e) Toy, P. H.; Newcomb, M.; Hollenberg, P. F. *J. Am. Chem. Soc.* **1998**, *120*, 7719–7729 and references therein.
- (2) (a) Yachandra, V. K.; Sauer, K.; Klein, M. P. *Chem. Rev.* **1996**, *96*, 2927–2959. (b) *Oxygenic Photosynthesis: The Light Reactions*; Ort, D. R., Yocum, C. F., Eds.; Kluwer Academic: The Netherlands, 1996. (c) Hoganson, C. W.; Babcock, G. T. *Science* **1997**, *277*, 1953–1956.
- (3) Selected examples: (a) Karlin, K. D.; Gultneh, Y. *Prog. Inorg. Chem.* **1987**, *35*, 219–328. (b) Karlin, K. D.; Tyeklár, Z.; Zuberbühler, A. D. In *Bioinorganic Catalysis*; Reedijk, J., Ed.; Marcel Dekker: New York, 1993; pp 261–315. (c) Kitajima, N.; Moro-oka, Y. *Chem. Rev.* **1994**, *94*, 737–757. (d) Que, L., Jr.; Dong, Y. *Acc. Chem. Res.* **1996**, *29*, 190–196. (e) Que, L., Jr. *J. Chem. Soc., Dalton Trans.* **1997**, 3933–3940. (f) Groves, J. T.; Han, Y.-Z. In ref 1b, pp 3–48. (g) Tolman, W. B. *Acc. Chem. Res.* **1997**, *30*, 227–237. (h) Karlin, K. D.; Kaderli, S.; Zuberbühler, A. D. *Acc. Chem. Res.* **1997**, *30*, 139–147.

- (4) (a) Wallar, B. J.; Lipscomb, J. D. *Chem. Rev.* **1996**, *96*, 2625–2658. (b) Solomon, E. I.; Sundaram, U. M.; Machonkin, T. E. *Chem. Rev.* **1996**, *96*, 2563–2605. (c) Klinman, J. P. *Chem. Rev.* **1996**, *96*, 2541–2561. (d) For interesting discussions of this and other related issues as they pertain to soluble methane monooxygenase, see the Commentaries by various authors in *J. Biol. Inorg. Chem.* **1998**, *3*, 300–336.
- (5) (a) Halfen, J. A.; Mahapatra, S.; Wilkinson, E. C.; Kaderli, S.; Young, V. G., Jr.; Que, L., Jr.; Zuberbühler, A. D.; Tolman, W. B. *Science* **1996**, *271*, 1397–1400. (b) Equilibration between (μ - η^2 : η^2 -peroxo)- and bis(μ -oxo)dicopper cores supported by a bis(pyridyl)amine ligand was implicated recently: Obias, H. V.; Lin, Y.; Murthy, N. N.; Pidcock, E.; Solomon, E. I.; Ralle, M.; Blackburn, N. J.; Neuhold, Y.-M.; Zuberbühler, A. D.; Karlin, K. D. *J. Am. Chem. Soc.* **1998**, *120*, 12960–12961.

Scheme 1



Scheme 1]⁶ and $[(\text{L}^{\text{Pr}^3}\text{Cu})_2(\mu\text{-O})_2]\text{X}_2$ [2(X)_2]. Kinetic evidence using stopped-flow methods supported equilibration of $\text{1(SbF}_6)_2$ and $\text{2(SbF}_6)_2$ that is more rapid than the initial O_2 binding step.^{5a} In a key experiment that demonstrated the capability of cores A and B to interconvert, addition of a large volume of THF (50-fold excess) to a 1.2 mM solution of $\text{1(ClO}_4)_2$ in CH_2Cl_2 (where it predominates) induced its conversion to $\text{2(ClO}_4)_2$, while the reverse addition of CH_2Cl_2 to a 1.2 mM solution of solely $\text{2(ClO}_4)_2$ in THF generated $\text{1(ClO}_4)_2$ (Figure S1, Supporting Information).^{5a}

Surprised by this abrupt isomerization process and motivated by its potential importance as a model for dioxygen-forming and -consuming reactions in Nature, we have endeavored to understand how simply changing the composition of the solvent induces it. While the above evidence supported rapid equilibration of $\text{1(SbF}_6)_2/\text{2(SbF}_6)_2$ in acetone, the existence of such an equilibrium in CH_2Cl_2 and/or THF solution has been less clear due to numerous complicating factors (vide infra). In this contribution we describe results of experiments aimed at addressing these issues and, ultimately, at understanding more completely the thermodynamics of and environmental influences on the $\text{1(X)}_2/\text{2(X)}_2$ interconversion. Importantly, conditions were found that enabled the identification and characterization of the homogeneous $\text{1(X)}_2/\text{2(X)}_2$ equilibrium in THF, in various THF/ CH_2Cl_2 mixtures, and at different temperatures. The observed gradual changes in the proportions of the cores A and B in these dicopper complexes as a function of solvent and temperature reflect subtle environmental effects on their relative stability, with attendant implications for their involvement in biology and catalysis.

Results

Several issues complicated previous efforts to unambiguously identify and characterize an equilibrium between 1(X)_2 and 2(X)_2 in CH_2Cl_2 , THF, or mixtures of these solvents. Previously, we had no evidence for the presence of $\text{1(ClO}_4)_2$ in THF solution (where only $\text{2(ClO}_4)_2$ was seen; Table 1), but UV-vis and resonance Raman data in CH_2Cl_2 (where $\text{1(ClO}_4)_2$ dominated) did contain features of weak intensity possibly attributable to $\text{2(ClO}_4)_2$ [cf. the shoulder at ~ 400 nm marked by an asterisk alongside the main band at 366 nm for $\text{1(ClO}_4)_2$ in Figure S1]. Nonetheless, we were puzzled by the observation that the λ_{max} for the longest wavelength absorption of what appeared to be $\text{2(ClO}_4)_2$ when a minor component in this case (as well as in

acetone)^{5a} is clearly shifted by >25 nm to shorter wavelength than when it is the only species present in THF. Attempts to more directly assess the solvent effects on the relative stability of 1(X)_2 and 2(X)_2 by analyzing spectra of mixtures of THF and CH_2Cl_2 at ratios intermediate between those used in the original experiment (Figure S1) also led to confusing results.⁷ For example, contrary to expectations for a simple equilibrium, in experiments with Cu(I) precursor concentrations ≥ 2 mM the $\text{1(X)}_2:\text{2(X)}_2$ ratio depended on the order of solvent mixing used to generate the intermediate solvent ratios (dilution of a CH_2Cl_2 solution with THF vs the opposite). Further complicating the interpretation of solvent-mixing experiments, large baseline absorptions in UV-vis spectra of ≥ 2 mM solutions of 2(X)_2 ($\text{X} = \text{ClO}_4^-$ or PF_6^-) in pure THF (Figure S1) correlated with turbidity observable by eye.

To address these issues, the oxygenation of $[\text{L}^{\text{Pr}^3}\text{Cu}(\text{CH}_3\text{CN})]\text{X}$ ($\text{X} = \text{PF}_6^-$, ClO_4^- , or SbF_6^-) was studied using a modified apparatus that allowed simultaneous bubbling of O_2 and acquisition of UV-vis spectral data at low temperatures (see Experimental Section). In most experiments, ligand with perdeuterated isopropyl substituents ($d_{21}\text{-L}^{\text{Pr}^3}$) was used in order to slow decomposition of the $\mu\text{-}\eta^2\text{:}\eta^2\text{-peroxo-}$ and/or bis($\mu\text{-oxo-}$)dicopper products that were shown previously to decay via rate-controlling scission of the isopropyl methine C-H bond with a large H/D kinetic isotope effect.^{8,9} In initial experiments we focused on using varying concentrations of complex in pure THF.

The Peroxo/Bis($\mu\text{-oxo}$) System in THF. In contrast to previous work that showed that 2.4 mM solutions of the Cu(I) precursor ($\text{X} = \text{PF}_6^-$ or ClO_4^-) in THF generated only 2(X)_2 (Figure S1), at lower concentrations time dependent behavior was observed with these counterions. As shown in Figure 1, in the first 4 min of oxygenation of a 0.28 mM solution of Cu(I) complex at -60 °C (here with $\text{X} = \text{PF}_6^-$), spectral features consistent with generation of a mixture of 1(X)_2 (major) and 2(X)_2 (minor) grow in. The feature with $\lambda_{\text{max}} = 364$ nm is due to peroxo complex 1(X)_2 , and the shoulder at longer wavelength is attributed to 2(X)_2 . These features change at longer times (vide infra), but for $\text{X} = \text{SbF}_6^-$, the same spectrum is obtained at higher concentrations of starting material (up to 1 mM) and it remains unperturbed until decomposition becomes significant (>1 h at -60 °C). Peak fitting of the spectrum for $\text{X} = \text{SbF}_6^-$ to mixed Gaussian/Lorentzian curves (see Experimental Section for details) yielded $\lambda_{\text{max}} = 418$ nm for the longer wavelength feature (Figure S2, Supporting Information), which is shifted 30 nm from the value previously reported^{5a} for more concentrated THF solutions (448 nm, Figure S1, Table 1). Consistent with previous results from stopped-flow experiments in acetone that supported rapid equilibration between $\text{1(SbF}_6)_2$ and $\text{2(SbF}_6)_2$,^{5a} their absorption bands also grow in at identical rates in THF. This is shown in the inset to Figure 1, where the absorbance as a function of time is plotted at 366 and 448 nm.¹⁰ Also shown is an exponential fit ($R = 0.998$) to the 366 nm data that yields a pseudo-first-order rate constant for the oxygenation of $k = 1.3 \times 10^{-2} \text{ s}^{-1}$, under conditions of O_2 saturation (we do not know the exact $[\text{O}_2]$ in THF at -60 °C). This rate constant is

- (7) Halfen, J. A.; Mahapatra, S.; Tolman, W. B. Unpublished results.
 (8) Mahapatra, S.; Halfen, J. A.; Tolman, W. B. *J. Am. Chem. Soc.* **1996**, *118*, 11575–11586.
 (9) Mahapatra, S.; Young, V. G., Jr.; Tolman, W. B. *Angew. Chem., Int. Ed. Engl.* **1997**, *36*, 130–133.
 (10) Although the λ_{max} value for the shoulder in Figure 1 was shown by peak fitting to be 418 nm, single-wavelength monitoring at 448 nm for comparing rates of oxygenation and decay (as in the inset to Figure 1) was more convenient for alleviating complications associated with overlap with absorbance from the 366 nm band.

(6) Mahapatra, S.; Halfen, J. A.; Wilkinson, E. C.; Que, L., Jr.; Tolman, W. B. *J. Am. Chem. Soc.* **1994**, *116*, 9785–9786.

Table 1. Selected Spectroscopic Properties of the Oxygenation Products Discussed in the Text

entry	ligand	anion	solvent	concn (mM) ^a	λ_{\max} (nm)				resonance Raman (cm ⁻¹) ^b		composition	ref
					1	2	3	4	$\nu(\text{Cu}_2\text{O}_2)$	$\nu(\text{O}-\text{O})$		
1	L ^{iPr3}	ClO ₄	CH ₂ Cl ₂	2.4		366		510		714 ^c	peroxo	5
2	L ^{iPr3}	ClO ₄	THF	2.4	324		448		589 ^d		bis(oxo)	5
3	L ^{iPr3}	SbF ₆	acetone	0.63	<i>e</i>	366	415	510	594 ^d	714 ^c	mixture	5
4	<i>d</i> ₂₁ -L ^{iPr3}	SbF ₆	<i>d</i> ₈ -THF	0.3	<i>f</i>	364	418	510	589	<i>g</i>	mixture	this work
5	L ^{iPr3}	SbF ₆	THF	2.0	<i>f</i>	364	418	510		711	mixture	this work
6	L ^{iPr3}	PF ₆	acetone	4.0	<i>e</i>	366	415	510	592	715	mixture	13
7	<i>d</i> ₂₁ -L ^{iPr3}	PF ₆	THF	0.28 ⁱ	<i>f</i>	366	418	510			mixture	this work
8	<i>d</i> ₂₁ -L ^{iPr3}	PF ₆	THF	0.28 ^j		324		448			bis(oxo)	this work
9	L ^{Bn3}	ClO ₄	CH ₂ Cl ₂			318		430		603/595 ^k	bis(oxo)	12,13
10	Tp ^{iPr2}		acetone				389	551		741	peroxo	18
11	His		oxyhemocyanin				340	580		748	peroxo	4b
12	His		oxytyrosinase				345	600		750	peroxo	4b
13	His		catechol oxidase				343	580		750	peroxo	27

^a Cu(I) precursor concentration for UV-vis samples and, for entries 4–6, for resonance Raman samples. ^b Only modes attributable to the symmetric vibration of the bis(μ -oxo)dicopper core [$\nu(\text{Cu}_2\text{O}_2)$] or the O–O stretching mode of the (μ - η^2 : η^2 -peroxo)dicopper core [$\nu(\text{O}-\text{O})$] are listed. Excitation wavelengths $\lambda_{\text{ex}} = 457.9$ nm and/or $\lambda_{\text{ex}} = 514.5$ nm were used, with greatest enhancement of the $\nu(\text{O}-\text{O})$ feature being observed with the latter. ^c Corrected from originally reported value of 722 cm⁻¹ (see ref 13). ^d Corrected from originally reported value of 602 cm⁻¹ (see ref 13). ^e Obscured by solvent absorption. ^f Peak fitting suggests a band at ~ 300 nm, but this peak is not well-resolved from the strong 366 nm absorption of the peroxo species. ^g Obscured by solvent band at 707 cm⁻¹. ^h Obscured by solvent band at 588 cm⁻¹. ⁱ Early oxygenation time (0–4 min, Figure 1); resonance Raman spectra not measured. ^j Late oxygenation time (after 20 min, Figure 3); resonance Raman spectra not measured. ^k Fermi doublet (ref 13).

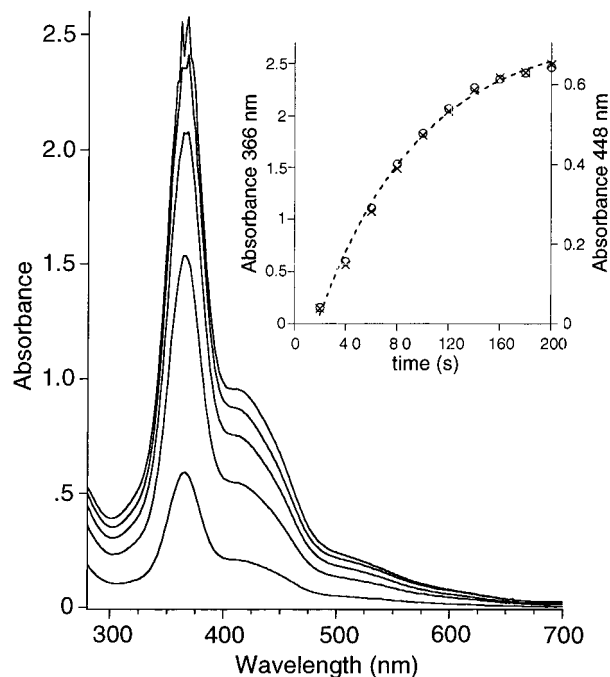


Figure 1. UV-vis spectra acquired every 40 s during the first 4 min of the oxygenation of $[\text{L}^{\text{iPr}_3}\text{Cu}(\text{CH}_3\text{CN})]\text{PF}_6$ (0.28 mM) in THF at -60 °C. The inset shows the time course of the absorbance at 366 nm (x) and 448 nm (o) with an exponential fit to the 366 nm data (dashed line).

in reasonable agreement with the data previously reported using stopped-flow methods in acetone if we assume roughly similar $[\text{O}_2]$ in the two different solvents.^{5a,11}

To confirm that the spectra in Figure 1 correspond to a mixture of $\mathbf{1}(\text{X})_2$ and $\mathbf{2}(\text{X})_2$ and, thus, alleviate our concern that the compound giving rise to the band with $\lambda_{\text{max}} = 418$ nm might be different from that with $\lambda_{\text{max}} = 448$ nm that was shown

conclusively to be $\mathbf{2}(\text{X})_2$ in previous work,^{5a,12} we turned to resonance Raman (RR) spectroscopy as an additional characterization technique. Samples were oxygenated under conditions identical to those used in the experiments monitored by UV-vis spectroscopy, except after the appropriate time an aliquot was flash frozen on a precooled gold-plated copper coldfinger for RR analysis. We were unable to verify the presence of both $\mathbf{1}(\text{X})_2$ and $\mathbf{2}(\text{X})_2$ in a single experiment because their respective diagnostic features were partially obscured by those due to solvent (THF has a band at 707 cm⁻¹ close to where the peroxo $\nu(\text{O}-\text{O})$ would be expected, while *d*₈-THF has a band at 588 cm⁻¹ near the anticipated position of the $[\text{Cu}_2(\mu\text{-O})_2]^{2+}$ core mode). Thus, each species was identified in separate experiments. The RR spectrum obtained for the complex of ligand with perdeuterated iPr groups and $\text{X} = \text{SbF}_6^-$ in *d*₈-THF (0.3 mM) using $\lambda_{\text{ex}} = 457.9$ nm is shown in Figure 2a. This spectrum clearly indicates the presence of the bis(μ -oxo)dicopper core; the vibration of the core is seen at 589 cm⁻¹, with the other peaks being due to ligand-based vibrations as will be described in more detail elsewhere. Importantly, the spectrum is identical to that obtained with more concentrated THF solutions with $\text{X} = \text{ClO}_4^-$ that by UV-vis and EXAFS spectroscopy contain only the bis(μ -oxo)dicopper core, but with $\lambda_{\text{max}} = 448$ nm.^{5a,9} In a separate experiment using fully protiated THF and L^{iPr3}, $\lambda_{\text{ex}} = 514.5$ nm, and $\text{X} = \text{SbF}_6^-$, a peak due to the O–O stretch of the peroxo complex $\mathbf{1}(\text{SbF}_6)_2$ is seen at 711 cm⁻¹ (Figure 2b).¹³ For comparison, the RR spectrum of the mixture of $\mathbf{1}(\text{PF}_6)_2$ and $\mathbf{2}(\text{PF}_6)_2$ generated in acetone is shown in Figure 2c;¹³ the features here and those obtained with $\text{X} = \text{SbF}_6^-$ in THF and *d*₈-THF, respectively (Figure 2a,b), closely correspond. Data collected for $\text{X} = \text{PF}_6^-$ in acetone solution that was frozen at -196 °C or still fluid at -80 °C (Figure S3, Supporting Information) were essentially the same, providing further support

(11) The second-order rate constant determined in the stopped-flow experiments $k = 1.77 \text{ M}^{-1} \text{ s}^{-1}$ was measured using $[\text{Cu}(\text{I})] = 6.3 \times 10^{-4} \text{ M}$ and $[\text{O}_2] = 5.1 \times 10^{-3} \text{ M}$ in acetone at -60 °C.^{5a} This corresponds to a pseudo-first-order (excess O₂) rate constant $k = 0.9 \times 10^{-2} \text{ s}^{-1}$, quite close to the value of $1.3 \times 10^{-2} \text{ s}^{-1}$ that we have measured in THF solution.

(12) Mahapatra, S.; Halfen, J. A.; Wilkinson, E. C.; Pan, G.; Wang, X.; Young, V. G., Jr.; Cramer, C. J.; Que, L., Jr.; Tolman, W. B. *J. Am. Chem. Soc.* **1996**, *118*, 11555–11574.

(13) The value for the peroxo $\nu(\text{O}-\text{O})$ is ~ 7 – 10 cm^{-1} lower in frequency than reported in previous studies (e.g., refs 5, 12). As will be described in full in a separate account, these previous reports were found subsequently to have used an incorrect solvent calibration. The correct frequencies for $\mathbf{1}(\text{PF}_6)_2$ and $\mathbf{2}(\text{PF}_6)_2$ in acetone are shown in Figure 2c and are listed in Table 1; the correct core vibration for $\mathbf{2}(\text{ClO}_4)_2$ in concentrated THF is 589 cm⁻¹.

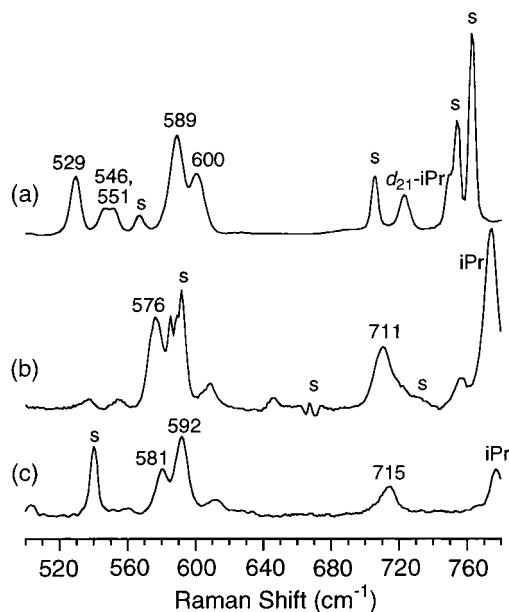
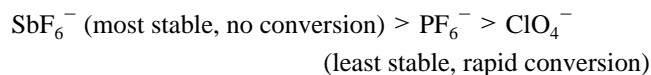


Figure 2. (a) RR spectrum using $\lambda_{\text{ex}} = 457.9$ nm of $[d_{21}\text{-LiPr}_3\text{Cu}(\text{CH}_3\text{CN})]\text{SbF}_6$ in $d_8\text{-THF}$ (0.3 mM) after oxygenation at -60 °C for 10 min. (b) RR spectrum with solvent bands subtracted using $\lambda_{\text{ex}} = 514.5$ nm of $[\text{LiPr}_3\text{Cu}(\text{CH}_3\text{CN})]\text{SbF}_6$ in THF (2 mM) after oxygenation at -70 °C for 10 min. (c) RR spectrum using $\lambda_{\text{ex}} = 514.5$ nm of $[\text{LiPr}_3\text{Cu}(\text{CH}_3\text{CN})]\text{SbF}_6$ in acetone after oxygenation at -70 °C for ~ 20 min. In all spectra, "s" denotes peaks due to solvent. Note that the peak in spectrum a at 600 cm^{-1} is due to perdeuteration of LiPr_3 (to be described more fully elsewhere).

for attribution of the bis(μ -oxo)dicopper core vibration to the species giving rise to the λ_{max} at 418 nm. In sum, RR spectroscopy confirms that the THF solutions of the complexes at early oxygenation times (low concentration, $\text{X} = \text{ClO}_4^-$ or PF_6^-) or at longer times (range of concentrations, $\text{X} = \text{SbF}_6^-$) that give rise to the UV-vis features shown in Figure 1 contain a mixture of $1(\text{X})_2$ and $2(\text{X})_2$ similar to that seen in acetone.^{5a}

Unlike in acetone solution, however, the UV-vis spectral features of the mixture of $1(\text{X})_2$ and $2(\text{X})_2$ in THF (0.28 mM in copper, $\text{X} = \text{ClO}_4^-$ or PF_6^-) transform upon standing at -60 °C. The changes observed in the 4–20 min time regime in an illustrative experiment are shown in Figure 3. Simultaneously, the 366 nm band due to $1(\text{X})_2$ decreases, the 418 nm shoulder due to $2(\text{X})_2$ appears to shift to 448 nm, a new peak at ~ 324 nm grows in, and the baseline rises. The concurrence of these changes is consistent with their association with a single physical and/or chemical process. An important additional observation was that the time at which these changes began depended upon the copper complex concentration and the nature of the counterion. The stability of the initially formed solution containing the $1(\text{X})_2/2(\text{X})_2$ mixture decreased as the concentration increased (i.e., the UV-vis changes occurred sooner) and followed the order for X



For the intermediate case of $\text{X} = \text{PF}_6^-$, by choosing a sufficiently low concentration of Cu(I) precursor (0.07 mM), conversion of the initially generated $1(\text{X})_2/2(\text{X})_2$ mixture could be inhibited almost completely (until very long times > 1.5 h).

The final spectrum in Figure 3 is essentially the same as previously reported for the bis(μ -oxo)dicopper complex $2(\text{ClO}_4)_2$ at high concentration (2.8 mM in copper) in THF [except for the shoulder at 366 nm in Figure 3 due to a minor, residual

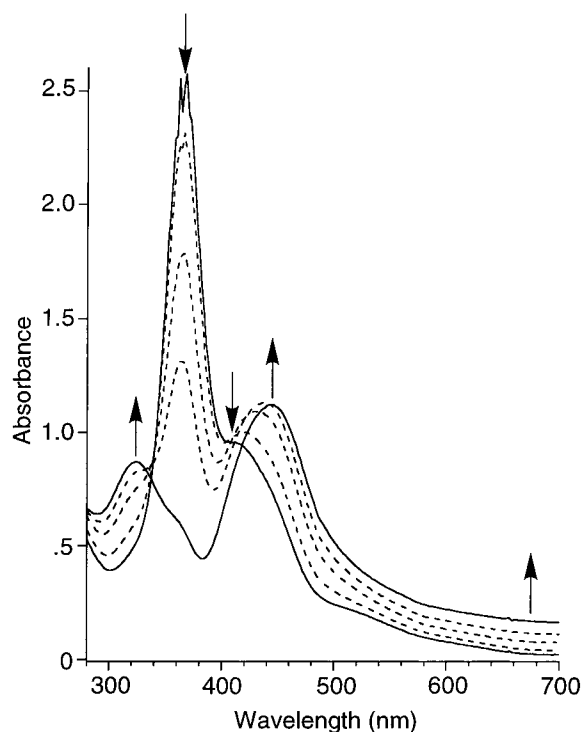


Figure 3. UV-vis spectra after 4 (solid line), 5, 6, 7 (all dashed lines), and 20 min (solid line) of oxygenating $[\text{LiPr}_3\text{Cu}(\text{CH}_3\text{CN})]\text{PF}_6$ (0.28 mM) in THF at -60 °C, with arrows denoting the growth and decay of features described in the text.

amount of $1(\text{X})_2$].^{5a,12} Thus, it appears that the initial mixture composed of mostly $1(\text{X})_2$ with a smaller amount of $2(\text{X})_2$ converts entirely to $2(\text{X})_2$, but the λ_{max} shift of 30 cm^{-1} and the baseline increase indicate additional perturbations. We propose that these changes are due to preferential aggregation and/or precipitation of $2(\text{X})_2$, and that this phenomenon drives an initial (homogeneous) equilibrium between $1(\text{X})_2$ and $2(\text{X})_2$ toward the latter. That is, we attribute the baseline increase to light scattering by some type of aggregate/precipitate of $2(\text{X})_2$, which because of its change in physical form exhibits a shifted λ_{max} . At the low concentrations used in the above experiments visual identification of a precipitate was difficult (often, no turbidity was visible), although in some instances some cloudiness was seen. In a key experiment with $\text{X} = \text{PF}_6^-$ (0.3 mM in copper), the oxygenated solution was allowed to stand for an extended period (~ 3 h) at -60 °C, whereupon a gradual decrease in the absorbance of the entire transformed spectrum of $2(\text{PF}_6)_2$ coincided with deposition of a finely dispersed orange-brown powder. Subsequent shaking of the mixture (keeping the temperature below -60 °C to avoid decomposition) to generate a cloudy solution regenerated the original spectrum, including the high baseline, thus showing definitively that the feature with $\lambda_{\text{max}} = 448$ and the baseline absorption are due to precipitated $2(\text{PF}_6)_2$ in this case. The aforementioned dependence of the conversion onset time on concentration and counterion are also consistent with the aggregation/precipitation hypothesis; aggregation/precipitation occurs sooner at higher concentration, and because ionic species are involved, the nature of the counterions is influential.

To further test the aggregation/precipitation hypothesis, we measured the conductivity of solutions while simultaneously monitoring the oxygenation and subsequent processes by UV-vis spectroscopy. As expected, upon reaction of $[d_{21}\text{-LiPr}_3\text{Cu}(\text{CH}_3\text{CN})]\text{PF}_6$ in THF (0.30 mM) with O_2 to form the $1(\text{PF}_6)_2/2(\text{PF}_6)_2$ mixture at -74 °C, the conductance changed con-

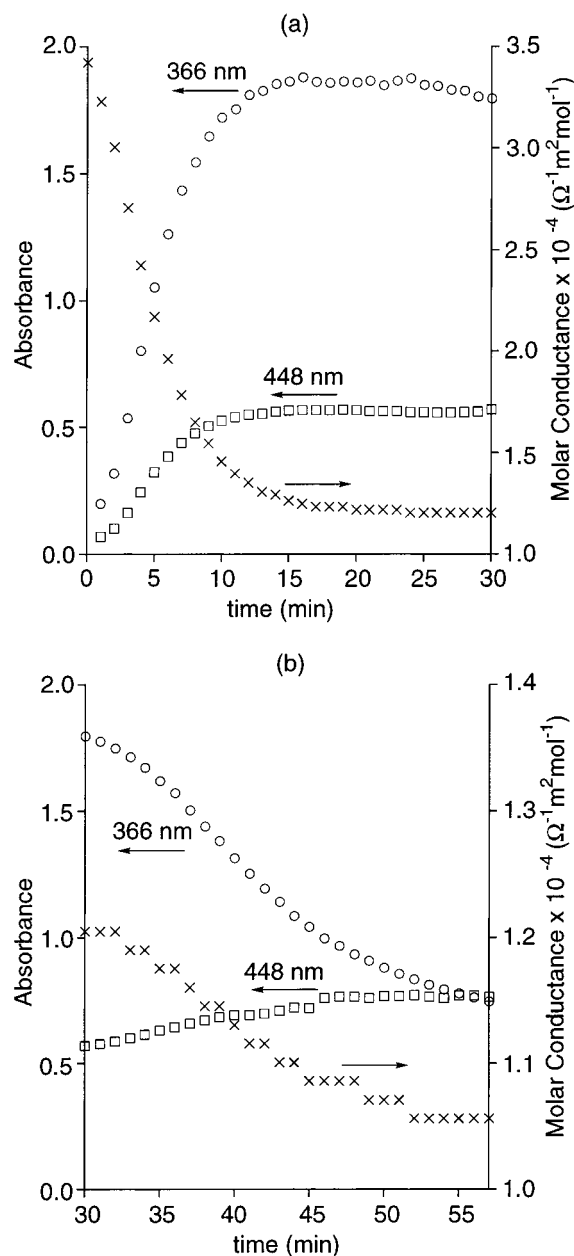


Figure 4. Plots of absorbance monitored at 366 (○) and 448 (□) nm and molar conductivity (×) measured simultaneously as a function of time during and after the oxygenation of $[\text{d}_{21}\text{-L}^{\text{iPr}_3}\text{Cu}(\text{CH}_3\text{CN})]\text{PF}_6$ in THF (0.30 mM) at $-74\text{ }^\circ\text{C}$. Note that the molar conductivity axis differs between plots a and b.

comitantly (Figure 4a). This result reflects the change from a 0.3 mM solution of a 1:1 electrolyte to a solution composed of a 1:2 electrolyte at 0.15 mM concentration. An increase in ion pairing upon oxygenation also may contribute to the large drop in conductivity. During the ensuing period (ca. 13–33 min, Figure 4a) when the homogeneous $1(\text{PF}_6)_2/2(\text{PF}_6)_2$ mixture was stable, the conductivity of the solution was unchanged. Importantly, at the onset of the conversion of the $1(\text{PF}_6)_2/2(\text{PF}_6)_2$ mixture to $2(\text{PF}_6)_2$ alone (apparent from the decay of the 366 nm absorption, shift of the 418 nm band to 448 nm, and growth of baseline absorbance), the conductivity also changed, albeit less dramatically than during the initial oxygenation (Figure 4b; note the change in the scale of the conductivity axis). Figure 4b shows that the drop in conductivity closely parallels the decay of the 366 nm band of $1(\text{PF}_6)_2$, and halts simultaneously with the UV–vis changes (~ 1 h). These findings are consistent with

the aggregation/precipitation hypothesis, although the small change in conductance is rather uninformative with respect to the nature of the aggregate(s).

A key element of the aggregation/precipitation idea is the postulate of a homogeneous equilibrium between $1(\text{X})_2$ and $2(\text{X})_2$ in THF at low concentrations/early times for $\text{X} = \text{PF}_6^-$ or ClO_4^- and at a range of concentrations for $\text{X} = \text{SbF}_6^-$. Such an equilibrium would be expected to exhibit a temperature dependence, with equilibrium constants at different temperatures that must not depend on how the equilibrium was reached (i.e., by warming or cooling). In a series of experiments designed to test these notions, 0.054 mM solutions of $[\text{d}_{21}\text{-L}^{\text{iPr}_3}\text{Cu}(\text{CH}_3\text{CN})]\text{SbF}_6$ in THF were oxygenated at different temperatures; the resulting UV–vis spectra are overlaid (after correction of the absorbances for solvent contraction)¹⁴ in Figure S4 (Supporting Information). The data show (a) a smooth shift of the relative intensities of the bands due to $1(\text{SbF}_6)_2$ and $2(\text{SbF}_6)_2$ with temperature and (b) an increase in the proportion of $2(\text{SbF}_6)_2$ as the temperature is lowered. Importantly, the spectra at the low and high temperatures were also obtained by oxygenating at the high and low temperatures, respectively, followed by shock cooling or warming of the solutions. These results represent key evidence confirming the existence of an equilibrium between $1(\text{X})_2$ and $2(\text{X})_2$ in THF. Similar results were seen for the system with $\text{X} = \text{PF}_6^-$ in acetone (data not shown).

Because we lack firm knowledge of the extinction coefficients (and their temperature dependencies) for $1(\text{SbF}_6)_2$ and $2(\text{SbF}_6)_2$ under the conditions used in the above experiments, accurate quantification of the temperature dependence of their ratio has not been possible. Still, approximations of the equilibrium constants at the different temperatures can be made if we estimate extinction coefficients per dicopper complex to be $22\,000\text{ cm}^{-1}\text{ M}^{-1}$ ($\lambda_{\text{max}} = 366\text{ nm}$) and $14\,000\text{ cm}^{-1}\text{ M}^{-1}$ ($\lambda_{\text{max}} = 414\text{--}424\text{ nm}$),¹⁵ reasonable values compared to those known for related systems.^{5,6,16} By comparing the peak heights of Gaussian/Lorentzian peak fits (Figures S5–S9, Supporting Information) to the overlapping bands due to $1(\text{SbF}_6)_2$ (366 nm) and $2(\text{SbF}_6)_2$ (414–424 nm)¹⁵ in the experimental spectra shown in Figure S4, $K_{\text{eq}} = [1(\text{X})_2]/[2(\text{X})_2]$ values were obtained. These are plotted as $\ln(K_{\text{eq}})$ vs T^{-1} in Figure S10 (Supporting Information), and a linear fit of the data ($R = 0.997$) provided the approximate thermodynamic parameters $\Delta H = 0.9(2)\text{ kcal mol}^{-1}$ and $\Delta S = 6(1)\text{ cal mol}^{-1}\text{ K}^{-1}$. Analogous treatment of the data for $\text{X} = \text{PF}_6^-$ in acetone (Figure S11, Supporting Information) gave similar values [$\Delta H = 0.7(2)\text{ kcal mol}^{-1}$ and $\Delta S = 5(1)\text{ cal mol}^{-1}\text{ K}^{-1}$]. At the risk of overinterpreting these crudely estimated parameters, the small enthalpy difference between $1(\text{X})_2$ and $2(\text{X})_2$ in THF or acetone agrees with the small energetic differences obtained from various theoretical calculations for related species with the same cores.¹⁷ Evaluating the entropy term is more difficult, as ill-understood contributions from solvation, ion pairing, etc. must be considered.

(14) Daubert, T. E. *Physical and Thermodynamic Properties of Pure Chemicals*; Hemisphere Publishing Corp.: New York, 1989; Vol. 1.

(15) As described in the Experimental Section and shown in Figures S5–S9 and S12–S17, the λ_{max} values for the fits to peak 3 [the low-energy bis(μ -oxo) CT] ranged from 414 nm ($-29\text{ }^\circ\text{C}$) to 424 nm ($-72\text{ }^\circ\text{C}$). Slight shifts also occur upon changing the concentration (cf. slightly different fits in Figures S5 and S12). These variations of $\leq 10\text{ nm}$ are relatively minor in view of the width at half-height of the peak ($\sim 75\text{ nm}$) and do not affect the major conclusions of this study.

(16) Mahadevan, V.; Hou, Z.; Cole, A. P.; Root, D. E.; Lal, T. K.; Solomon, E. I.; Stack, T. D. P. *J. Am. Chem. Soc.* **1997**, *119*, 11996–11997.

(17) (a) Cramer, C. J.; Smith, B. A.; Tolman, W. B. *J. Am. Chem. Soc.* **1996**, *118*, 11283–11287. (b) Liu, X.-Y.; Palacios, A. A.; Novoa, J. J.; Alvarez, S. *Inorg. Chem.* **1998**, *37*, 1202–1212. (c) Bérces, A. *Inorg. Chem.* **1997**, *36*, 4831–4837.

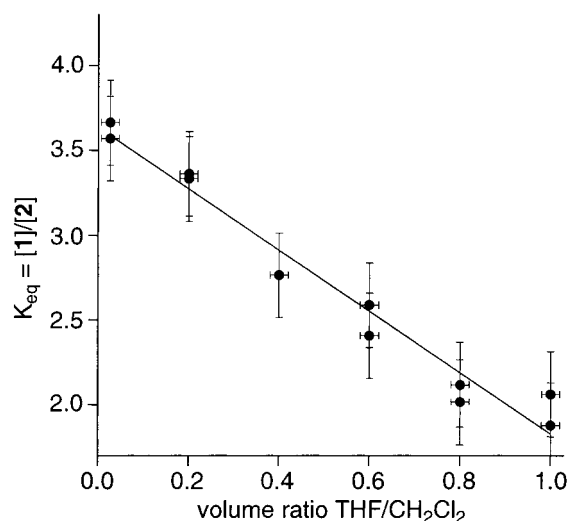


Figure 5. Plot of K_{eq} versus the volume ratio of THF and CH_2Cl_2 in mixtures of these two solvents. The K_{eq} values were estimated as described in the text from peak fits of replicate data shown in Figures S12–S17 for the oxygenation of 0.11 mM solutions of $[\text{d}_{21}\text{-L}^{\text{iPr}_3}\text{Cu}(\text{CH}_3\text{CN})]\text{SbF}_6$ at -60°C . A linear fit to the data is shown (slope = -1.81 ; $R = 0.982$).

Mixed Solvents. The discovery that the $1(\text{X})_2/2(\text{X})_2$ equilibrium shifts as a result of preferential aggregation/precipitation of $2(\text{X})_2$ under certain conditions led us to recognize this phenomenon as the source of previous difficulties in obtaining reproducible results in solvent-mixing experiments at intermediate solvent ratios. To avoid these problems, we oxygenated solutions of $[\text{d}_{21}\text{-L}^{\text{iPr}_3}\text{Cu}(\text{CH}_3\text{CN})]\text{SbF}_6$ in mixtures of THF and CH_2Cl_2 at low concentration (0.11 mM) with volume ratios ranging from 100% to 2.5% THF at -60°C . The spectra obtained from the separate experiments (Figures S12–S17, Supporting Information) indicate the presence of homogeneous mixtures of $1(\text{SbF}_6)_2$ and $2(\text{SbF}_6)_2$ in each case and, most significantly, a smooth increase in the relative amount of $2(\text{SbF}_6)_2$ as the proportion of THF is raised. Using peak fits to the data and the same estimated extinction coefficients as in the calculations above (with the same caveats), approximate K_{eq} values were calculated. When plotted versus the THF: CH_2Cl_2 volume ratio (Figure 5), a linear correlation between the solvent composition and K_{eq} is revealed.

Discussion

Using conductivity measurements and UV–vis and resonance Raman spectroscopy, we have examined important aspects of the solvent, counterion, and temperature dependence of the equilibrium between the $(\mu\text{-}\eta^2\text{-}\eta^2\text{-peroxo})$ - and bis($\mu\text{-oxo}$)-dicopper cores in a specific set of complexes, $1(\text{X})_2$ and $2(\text{X})_2$ (Scheme 1). To interpret the results, we relied heavily on previous work that established the spectroscopic signatures of these cores and correlated them to structural information from EXAFS and X-ray crystallographic studies.^{3g,5a,6,8,9,12,16} In a key finding, the previously reported formation of solely $2(\text{X})_2$ upon oxygenation of $[\text{L}^{\text{iPr}_3}\text{Cu}(\text{CH}_3\text{CN})]\text{X}$ ($\text{X} = \text{PF}_6^-$ or ClO_4^-) in THF or upon dilution with THF of concentrated solutions of $1(\text{X})_2$ in CH_2Cl_2 was found to result from its preferential aggregation/precipitation. At lower concentrations and early oxygenation reaction times with $\text{X} = \text{PF}_6^-$ or ClO_4^- , or by using $\text{X} = \text{SbF}_6^-$ at a range of concentrations, a homogeneous mixture of $1(\text{X})_2$ (major) and $2(\text{X})_2$ (minor) in equilibrium forms.

Several pieces of evidence support these postulates. The presence of the two isomers in the homogeneous mixture was

Table 2. Selected Physical Constants and Empirical Parameters for Solvents Used in This Study

parameter	acetone	CH_2Cl_2	THF
dielectric constant ^a	20.7	8.93	7.58
$E_T(30)$ (kcal mol ⁻¹) ^b	42.2	40.7	37.4
(normalized E_T^N) ^c	(0.355)	(0.309)	(0.207)
DN (kcal mol ⁻¹) ^d	17	0.0 ^e	20
$\Delta H_{\text{D-BF}_3}^\circ$ (kcal mol ⁻¹) ^f	18.2	2.4	21.6

^a Table A-1 in ref 22, pp 408–411. ^b Tables 7-3 in ref 23, pp 365–371. For definition see ref 21. ^c E_T^N are $E_T(30)$ values normalized to H_2O (1.00) and Me_4Si (0.00) by using the relationship $E_T^N = (E_T(30) - 30.7)/32.4$. See p 364 in ref 22. ^d Tables 2-3 in ref 22, pp 20–21. ^e This value corresponds to that for $\text{ClCH}_2\text{CH}_2\text{Cl}$, as we have been unable to locate a DN value for CH_2Cl_2 . ^f Tables 2-4 in ref 22, p 22.

confirmed by resonance Raman spectroscopy, which showed the diagnostic signatures of their respective cores [A_g vibration of the $[\text{Cu}_2(\mu\text{-O})_2]^{2+}$ rhomb¹³ and the peroxo $\nu(\text{O-O})$].¹⁸ Importantly, the bis($\mu\text{-oxo}$)-dicopper core vibration was the same in Raman spectra of the homogeneous mixture and of the final solution composed solely of $2(\text{X})_2$, despite differences in the λ_{max} for its lowest energy CT absorption band (418 vs 448 nm). This observation proves that the same molecular species comprising the bis($\mu\text{-oxo}$)-dicopper core gives rise to the different UV–vis absorptions. The selective aggregation/precipitation of $2(\text{X})_2$ ($\text{X} = \text{PF}_6^-$ or ClO_4^-) rationalizes this apparent dichotomy, especially when considered in conjunction with the corresponding (a) increase in the baseline of UV–vis spectra indicative of light scattering,¹⁹ (b) visible precipitate formation in some instances, (c) drop in conductance that closely parallels the UV–vis changes, and (d) dependence of the onset time on the concentration and the counterions, which somehow influence the solubility of $2(\text{X})_2$. Finally, the existence of an equilibrium between $1(\text{X})_2$ and $2(\text{X})_2$ in the homogeneous mixture prior to aggregation/precipitation is supported by (a) the observation by UV–vis spectroscopy of a smooth temperature dependence of the ratio of these two species and (b) the finding that these ratios can be reversibly perturbed by warming or cooling. Estimated thermodynamic parameters for this equilibrium are consistent with the small energy difference between the $(\mu\text{-}\eta^2\text{-}\eta^2\text{-peroxo})$ - and bis($\mu\text{-oxo}$)-dicopper cores calculated by various theoretical methods.¹⁷

The question of why $2(\text{X})_2$ aggregates/precipitates preferentially with respect to its isomer $1(\text{X})_2$ in concentrated THF solutions is difficult to address, particularly in view of the relatively subtle structural differences between the two similarly charged isomers.²⁰ Why this selective process does not occur in CH_2Cl_2 or acetone is also unresolved, although some insights are available from consideration of selected physical and empirical parameters for these solvents listed in Table 2. Note that the dielectric constants and empirical solvent polarity values $E_T(30)$ (and the normalized variant E_T^N)^{21,22} indicate a polarity

(18) (a) Kitajima, N.; Fujisawa, K.; Fujimoto, C.; Moro-oka, Y.; Hashimoto, S.; Kitagawa, T.; Toriumi, K.; Tatsumi, K.; Nakamura, A. *J. Am. Chem. Soc.* **1992**, *114*, 1277–1291. (b) Baldwin, M. J.; Root, D. E.; Pate, J. E.; Fujisawa, K.; Kitajima, N.; Solomon, E. I. *J. Am. Chem. Soc.* **1992**, *114*, 10421–10431. (c) Solomon, E. I.; Tuczek, F.; Root, D. E.; Brown, C. A. *Chem. Rev.* **1994**, *94*, 827–856.

(19) Particle size estimation by light-scattering measurements would be of interest, but technical difficulties have forestalled these experiments so far.

(20) While differences in the “ $\text{L}^{\text{iPr}_3}\text{Cu}$ ” portions of the structures of $2(\text{X})_2$ and $1(\text{X})_2$ probably are relatively insignificant, the overall dicationic portion of $2(\text{X})_2$ is more compact than that of $1(\text{X})_2$ due to its shorter Cu–Cu distance (2.8 vs 3.6 Å). Differences in the specific interactions of these differently sized dicationic cores with their counterions may be responsible for their contrasting behavior in concentrated THF solution, but we can only speculate as to the nature of these effects.

trend: acetone > CH₂Cl₂ > THF, with the similar $E_T(30)$ values in particular for CH₂Cl₂ and acetone being suggestive of similar polar behavior for these two solvents in a number of physical processes.²³ Thus, we ascribe the observation of aggregation/precipitation phenomena in THF but not in acetone or CH₂Cl₂ to the greater effective polarity of the latter two solvents that results in higher solubility for both **1**(X)₂ and **2**(X)₂. The ability of the solvents to act as electron pair donors does not appear to correlate with the observed solubility behavior, since the donor numbers (DN)²⁴ and related parameters $\Delta H^\circ_{D-BF_3}$ ²⁵ are similar for acetone and THF, with both being much larger than those for CH₂Cl₂.

With knowledge of the conditions under which selective aggregation/precipitation of **2**(X)₂ (X = PF₆⁻ or ClO₄⁻) may be avoided, we were able to unmask the effects of varying the solvent composition of THF/CH₂Cl₂ mixtures on the homogeneous **1**(X)₂/**2**(X)₂ equilibrium. In contrast to the discontinuous interconversion of **1**(X)₂ and **2**(X)₂ seen previously in solvent-mixing experiments performed at high concentrations (Figure S1, Supporting Information), a smooth variation of the proportion of these molecules with the THF:CH₂Cl₂ ratio was observed upon oxygenations of Cu(I) precursor solutions at lower concentrations; K_{eq} decreases as the THF:CH₂Cl₂ ratio increases (Figure 5). In an attempt to rationalize the greater relative stability of **2**(X)₂ as the proportion of THF is increased, we again turn to the data listed in Table 2. As discussed above, CH₂Cl₂ is more polar than THF, so a possible explanation may be that the shift to greater K_{eq} values as the proportion of CH₂Cl₂ increases results from the corresponding shift to a more polar medium. However, it is unclear why **1**(X)₂ would be preferentially stabilized by a more polar solvent mixture, and this notion goes against the results of theoretical calculations—admittedly with a system with different N-donor ligands—that showed that the bis(μ -oxo)dicopper core is relatively stabilized upon imposition of a continuum dielectric field.^{17a} An alternative explanation centers on the different electron pair donor/acceptor properties of CH₂Cl₂ and THF as reflected by their quite different DN and $\Delta H^\circ_{D-BF_3}$ values. Perhaps the greater proportion of **2**(X)₂ as the amount of THF is elevated is due to stabilizing interactions between the THF donor solvent molecules and the dicationic portion of **2**(X)₂, possibly via specific binding of THF solvent to its Cu(III) ions that are more highly oxidized and electrophilic than the Cu(II) ions of **1**(X)₂. The

greater electron pair donor capabilities of THF may also contribute to better nonspecific interactions with the ions and may increase the proportion of solvent-separated ion pairs, although it is not obvious why this should preferentially stabilize **2**(X)₂ relative to **1**(X)₂. The specific and nonspecific interactions of THF with **2**(X)₂ would be further accentuated at lower temperatures, thus rationalizing the observed temperature dependence of K_{eq} . Moreover, the similar behavior of acetone and THF (once the aggregation/precipitation phenomenon is avoided) coincides with their similar DN and $\Delta H^\circ_{D-BF_3}$ values. Still, further experiments with other solvent mixtures and counterions are needed to evaluate these hypotheses.

Concluding Remarks

The results of the experiments described herein provide important support for the existence of a rapid equilibrium between energetically similar complexes with (μ - η^2 : η^2 -peroxo)- and bis(μ -oxo)dicopper cores (**A** and **B**, M = Cu) when supported by the specific ligand L^{iPr3}. The observed gradual shifts in the relative proportion of the isomeric complexes as a function of solvent composition, identity of counterions, and temperature show that subtle environmental factors perturb this equilibrium in equally subtle ways.²⁶ Although theoretical calculations have corroborated these experimental results by showing that these cores (capped by different N-donor ligands) have similar energies and that the barrier for their interconversion is small, these calculations have neglected specific counterion, ligand substituent, and solvent effects that clearly are important.^{12,17} Future efforts to characterize this and related systems by theory should attempt to take these effects into account. Finally, the demonstration in a synthetic system that the proportion of **A** and **B** (M = Cu) can be sensitive to environmental factors has numerous important implications for oxidation processes in biology and industry. In a particularly pertinent example, although a (μ - η^2 : η^2 -peroxo)dicopper species is the only intermediate observed so far during turnover of tyrosinase,^{4b} which converts phenols to *o*-quinones, and catechol oxidase,²⁷ which transforms catechols to *o*-quinones, our findings raise the possibility that it may isomerize to a bis(μ -oxo) unit prior to attacking substrate. As suggested by this work, relatively minor perturbations of the active site environment and/or binding of phenol substrate may be sufficient to induce the **A** → **B** transformation in tyrosinase. Whether the latter actually is capable of hydroxylating an aromatic substrate thus becomes a critical issue that merits further study.

Experimental Section

General Procedures. All reagents and solvents were obtained from commercial sources and were used as received unless stated otherwise. Solvents were dried according to published procedures²⁸ and distilled under N₂ prior to use. Dioxygen gas was dried by passing through a short column of Drierite. All Cu(I) complexes were prepared as described previously,¹² and formulations for the new compounds [*d*₂₁-L^{iPr3}Cu(CH₃CN)]X, X = PF₆⁻ and SbF₆⁻, were corroborated by ¹H NMR spectroscopy and elemental analysis (CHN).

Physical Methods. Low-temperature UV–visible spectra were recorded on either a Hewlett-Packard HP8452A diode array spectro-

- (21) The $E_T(30)$ is the energy (kcal mol⁻¹) of the longest wavelength absorption band of 2,6-diphenyl-4-(2,4,6-triphenyl-1-pyridinio)phenoxide measured at 25 °C and 760 Torr. It is a useful empirical indicator of solvent polarity; the larger the $E_T(30)$ value, the greater the polarity of the solvent. See pp 363–374 in ref 22. It should be noted that the use of the values shown in Table 2 to characterize the systems described herein that were studied at temperatures < -30 °C should be accompanied by a caveat, since $E_T(30)$ values are sensitive to temperature. Thus, the absolute values are probably incorrect, but we expect the trends among the various solvents to remain relatively unchanged at the temperatures used in our experiments.
- (22) Reichardt, C. *Solvents and Solvent Effects in Organic Chemistry*, 2nd ed.; VCH: Weinheim, Germany, 1988.
- (23) It has been shown that $E_T(30)$ values correlate linearly with numerous solvent-sensitive processes including optical absorption, rates of reactions, and equilibrium constants, and do not always correlate with dielectric constants (pp 363–374 in ref 22).
- (24) The donor number (DN) is the negative ΔH value for 1:1 adduct formation between SbCl₅ and an electron-pair donor solvent in dilute ClCH₂CH₂Cl solution, as defined by the following: See ref 23 and Gutmann, V. *The Donor-Acceptor Approach to Molecular Interactions*; Plenum Press: New York, 1978.
- (25) The $\Delta H^\circ_{D-BF_3}$ is the standard molar enthalpy of 1:1 adduct formation between an electron pair donor solvent (D) and gaseous BF₃ in dilute CH₂Cl₂ at 25 °C. A caveat on the use of these values similar to that given in ref 22 should be noted. See pp 17–22 and 348 in ref 22.

- (26) Other factors also influence the proportion of **A** and **B** in analogous dicopper complexes, including the nature of the ligand substituents, the length of tethers linking the N-donor caps, and the macrocycle ring size.^{26a} (a) Lam, B.; Halfen, J. A.; Young, V. G., Jr.; Dixon, D.; Tolman, W. Unpublished results.
- (27) Eicken, C.; Zippel, F.; Büldt-Karentzopoulos, K.; Krebs, B. *FEBS Lett.* **1998**, *436*, 293–299.
- (28) Perrin, D. D.; Armarego, W. L. F. *Purification of Laboratory Chemicals*; Pergamon Press: New York, 1988.

photometer (190–820 nm scan range) or a Hewlett-Packard HP8453 diode array spectrophotometer (190–1100 nm scan range) using a custom-manufactured vacuum dewar equipped with quartz windows. To achieve and maintain low temperatures a copper-tubing coil was inserted into the methanol-filled UV–visible dewar through which cold methanol was circulated from an external source (Neslab cryocool system: CC-100 II immersion cooler, Agitainer, and Cryotrol temperature controller or ULT-80 low-temperature bath/circulator). The UV–vis dewar bath temperature was monitored using a resistance thermocouple probe (Fluke 51 K/J thermometer); close correspondence (± 0.2 °C) between the bath temperature and the temperature of the solution inside the cuvette was confirmed using the same thermometer. Resonance Raman spectra obtained at -196 °C were collected on an Acton 506 spectrometer using a Princeton Instruments LN/CCD-1100-PB/UVAR detector and ST-1385 controller interfaced with Winspec software. A Spectra-Physics 2030-15 argon ion laser at a power of roughly 30 mW was employed to give excitation at 514.5 or 457.9 nm. The spectra were obtained using a 135° backscattering geometry; samples were frozen onto a gold-plated copper coldfinger in thermal contact with a dewar containing liquid nitrogen. Solution resonance Raman spectra were collected at -80 °C using 406.7 nm radiation. Low temperature was achieved in a homemade cryostat in which a spinning NMR sample tube was cooled by liquid nitrogen boiloff. The temperature of the solution (prepared as described below) was maintained to ± 1 °C by an in-line resistive heater whose current was controlled by a PID temperature controller. The spectrometer used for scattered light collection, filtering, dispersion, and detection was previously described.²⁹ Raman shifts were referenced to the intense solvent feature at 667 cm^{-1} (THF), 837 cm^{-1} (d_8 -THF), 797 cm^{-1} (frozen acetone), or 786 cm^{-1} (acetone at -80 °C). Conductance measurements were performed using a YSI Model 35 conductance meter and a Model 31 conductivity bridge, the glass casing of which was modified to allow insertion into the UV–vis cell.

Oxygenation Reactions. Dry O_2 was bubbled through a precooled solution prepared from a stock solution of $[\text{L}^{\text{iPr}_3}\text{Cu}(\text{CH}_3\text{CN})]\text{ClO}_4$ or $[(d_{21}\text{-iPr}_3\text{TACN})\text{Cu}(\text{CH}_3\text{CN})]\text{X}$ ($\text{X} = \text{PF}_6^-$ or SbF_6^-) in CH_2Cl_2 , THF, or a mixture of CH_2Cl_2 and THF through a cannula inserted into one side of the UV–vis cell so that the light beam could pass through the other side without interference, thus allowing UV–vis and/or conductance monitoring as the oxygenation proceeded. Samples for resonance Raman spectroscopy at -196 °C were prepared by bubbling dry dioxygen through the appropriate precooled solution for 10 min, after which a drop of the resulting colored solution was transferred to and subsequently frozen onto a precooled gold-plated copper coldfinger. An aliquot of the solution also was transferred to a precooled UV–vis cell for comonitoring by UV–vis spectroscopy.

Peak Fitting. Peak fitting was performed using PeakSolve from Galactic Industries Corporation. Variable parameters in the peak-fitting

routine are the position of the peak center, peak height, peak width, and % Gaussian/Lorentzian peak shape. To obtain estimates of the ranges of values for these parameters for the solutions of $1(\text{X})_2$ and/or $2(\text{X})_2$, we examined pure solutions containing either the $(\mu\text{-}\eta^2\text{:}\eta^2\text{-peroxo})$ - or bis($\mu\text{-oxo}$)dicopper cores supported by N-donor ligands different from L^{iPr_3} . Specifically, we fitted ($R > 0.997$) the features at 381 nm (peak 2) and 534 nm (peak 4) in the spectrum of $[(\text{iPr}_3\text{TACD})_2\text{Cu}_2(\mu\text{-}\eta^2\text{:}\eta^2\text{-O}_2)](\text{SbF}_6)_2$ ($\text{iPr}_3\text{TACD} = 1,4,7\text{-triisopropyl-1,4,7-triazacyclodecane}$; Figure S18, Supporting Information)^{26a} and the features at 305–321 nm (peak 1) and 406–437 nm (peak 3) in the spectra of the bis($\mu\text{-oxo}$)dicopper complexes supported by 1,4,7-tribenzyl-1,4,7-triazacyclodecane,^{26a} 1,4,7-trimethyl-1,4,7-triazacyclodecane,^{26a} 1,4,7-tribenzyl-1,4,7-triazacyclononane, and 1,4-diisopropyl-7-benzyl-1,4,7-triazacyclononane (Figures S19–S22, Supporting Information).¹² From these fits it was determined (a) to use a 50% Gaussian/Lorentzian curve for all peaks, (b) to restrict the peak widths (at half-height) to the ranges 45–66 nm (peak 1), 37–45 nm (peak 2), 45–75 nm (peak 3), and 70–90 nm (peak 4), (c) to allow the peak center (λ_{max}) to vary within the ranges 295–316 nm (peak 1), 360–370 nm (peak 2), 414–424 nm (peak 3), and 500–520 nm (peak 4), and (d) to allow the peak height to vary freely. The varying values ultimately obtained for these parameters in the fits reflects subtle temperature and/or solvent effects on the absorption spectral features. While these complicate quantitative analysis (e.g., accuracy of K_{eq} values that are based on extinction coefficient estimates), they nonetheless had little impact on the major conclusions of this study. Other protocols were attempted (e.g., allowing the peak widths and/or % Gaussian/Lorentzian to vary freely), but these gave poorer fits. Importantly, if fixed values for the peak centers or peak widths were used, poor fits to the variable temperature (Figure S5–S9) or solvent mixture (Figure S12–S17, Supporting Information) data were obtained.

Acknowledgment. We thank the NIH (GM47365), the NSF (National Young Investigator Award to W.B.T., REU support to J.C.), the Beckman Foundation (Undergraduate Research Grant to J.C.), and the University of Minnesota (Lando Endowment and Undergraduate Research Opportunities Program grants to J.C.) for financial support of this research. We also thank Prof. Lawrence Que, Jr. (UM), and Prof. Kenton Rodgers (North Dakota State University) for providing access to Raman instrumentation, Prof. Louis Pignolet for assistance with the conductivity experiments, and Prof. Richard Finke (Colorado State University) for helpful discussions.

Supporting Information Available: UV–vis and solution resonance Raman data and fits and plots of K_{eq} vs $1/T$. This material is available free of charge via the Internet at <http://pubs.acs.org>.

(29) Lukat-Rodgers, G. S.; Rodgers, K. R. *Biochemistry* **1997**, *36*, 4178–4187.